Available online at www.sciencedirect.com
SCIENCE DIRECT®
Journal of Membrane Science 230 (2004) 71–89
journal of MEMBRANE SCIENCE
www.elsevier.com/locate/memsci

Modeling of asymmetric membrane formation by dry-casting method

Sacide Alsoy Altinkaya [a,*], Bulent Ozbas [b]

[a] *Department of Chemical Engineering, Izmir Institute of Technology, Gulbahce Koyu, Urla-Izmir 35437, Turkey*
[b] *Department of Materials Science and Engineering, Izmir Institute of Technology, Gulbahce Koyu, Urla-Izmir 35437, Turkey*

Received 14 January 2003; received in revised form 28 July 2003; accepted 8 October 2003

Abstract

Many polymeric membranes are produced by phase inversion technique invented by Loeb and Sourirajan in 1962. The dry-casting method is one of the major phase inversion techniques in which a homogeneous polymer solution consisting of solvent(s) and nonsolvent(s) is cast on a support and then evaporation of the casting solution takes place under convective conditions. In this paper, we model membrane formation by the dry-casting method. The model takes into account film shrinkage, evaporative cooling, coupled heat, and mass transfer and incorporates practical and reliable diffusion theory as well as complex boundary conditions especially at the polymer solution/air interface. The predictions from the model provide composition paths, temperature, and thickness of the solution. By plotting the composition paths on the ternary phase diagram, we ascertain the general structural characteristics of the membranes prepared from particular casting conditions. The predictive ability of the model was evaluated by comparing the results with the experimental data obtained from gravimetric measurements for cellulose acetate (CA)–acetone–water system. In an attempt to illustrate the importance of diffusion formalism on the predictions, recently proposed multicomponent diffusion theory and its simplified forms were utilized in the model. The computational results show that the critical factor for capturing the accurate behavior of membrane formation is the diffusion formalism utilized in the model.

Keywords: Asymmetric membrane; Dry-cast model; Multicomponent diffusion; Thermodynamics; Cellulose acetate

1. Introduction

The invention of the asymmetric membranes by Loeb and Sourirajan has made a great impact on the growth of membrane science and technology. This is due to the unique structure of these types of membranes comprising of a very thin, relatively dense skin layer supported by a more open porous sublayer. The permeability and high selectivity is imparted by the skin layer while the mechanical strength is provided by the porous sublayer. Based on specific application, desired purity of the permeate, and operating costs, structural characteristics of the membrane, such as fraction of the dense top layer and porous sublayer, size and shape of the pores, can be adjusted by optimizing the membrane preparation conditions. The optimization usually requires time consuming, extensive trial and error experimentation. This difficulty can be greatly overwhelmed by accurate and reliable mathematical models which guide us to understand and control membrane formation process and morphology.

Asymmetric membranes are mostly fabricated by a process called phase inversion, which can be achieved through four principal methods: immersion precipitation (wet-casting) [1–4], vapor-induced phase separation [5,6], thermally-induced phase separation [2,7], and dry-casting [8]. In all these techniques, an initially homogeneous polymer solution thermodynamically becomes unstable due to different external effects and phase separates into polymer lean and polymer rich phases. The polymer-rich phase forms the matrix of the membrane, while the polymer-lean phase rich in solvents and nonsolvents, fills the pores.

Most of the experimental and theoretical work in the literature is focused on wet-cast and thermal cast processes. There are relatively few quantitative studies on the dry cast process, even though this technique offers some advantages compared to other phase inversion techniques. However, models related to the dry-cast process have been developed for evaporative casting of dense films from binary polymer solutions. In these models, one dimensional unsteady state diffusion of a volatile component is considered. The first

* Corresponding author. Tel.: +90-232-498-6273; fax: +90-232-498-6196.
E-mail address: sacidealsoy@iyte.edu.tr (S.A. Altinkaya).

0376-7388/$ – see front matter © 2003 Elsevier B.V. All rights reserved.
doi:10.1016/j.memsci.2003.10.034

predictive evaporative casting model was developed by Anderson and Ullman [9]. Their model assumes semi-infinite film thickness, constant specified surface concentration, negligible film shrinkage, and isothermal mass transfer. Some of these assumptions were relaxed in the model of Castellari and Ottani [10]. They considered finite film thickness, uniform film shrinkage, and variable surface concentration. However, they also assumed negligle temperature change in the film. In addition, both of these models utilized self diffusion coefficient rather than the mutual diffusion coefficient in the mass transfer equation. Krantz et al. [11] and Tsay and McHugh [12] improved these earlier models by incorporating mass transfer resistance in the gas phase and different semi-empirical correlations for the binary mutual diffusion coefficient. However, they still neglect the evaporative cooling effect. The first binary evaporative casting model that considers coupled heat and mass transfer was derived by Tantekin-Ersolmaz [13]. It was shown that the predictions of this model are valid at short evaporation times. In a subsequent study, Shojaie et al. [14] presented a fully predictive nonisothermal model that incorporates excess volume of mixing effects, mass transfer resistance in the gas phase, and a correlation for the binary diffusion coefficient. The predictions of this model for the instantaneous mass and temperature were found to be in good agreement with the experimental data. The first model on dry-casting method for a ternary mixture was developed by Shojaie et al. [15]. In their model, mass-transfer process was analyzed by incorporating excess volume of mixing effects. The change in thickness of the film was considered, and the temperature profiles within the solution and substrate were predicted by solving the unsteady-state heat-transfer equations. Their diffusion formalism uses a simplified form of Bearman's friction-based theory in which self diffusion coefficients are related to ternary mutual diffusivities through friction coefficients. Cellulose acetate (CA)/acetone/water was chosen as a model system, and self diffusion coefficients were predicted from Fujita's free volume theory. The water/acetone and acetone/cellulose acetate friction coefficients were obtained from available binary diffusion coefficients while the water/cellulose acetate friction coefficients were related to acetone/cellulose acetate friction coefficients. In constructing the phase diagram, and in defining the boundary condition at the solution–air interface, Flory-Huggins thermodynamic theory with variable interaction parameter was used. In a subsequent paper, Shojaie et al. investigated the effect of initial composition and casting thickness on the membrane structure and compared the measurement of the total mass loss and temperature with the model predictions [16]. In another paper, Matsuyama et al. [17] studied membrane formation and structure development by dry-cast process both experimentally and theoretically. In particular, various types of porous membranes were prepared by the dry-cast process in several cellulose acetate/acetone/nonsolvent systems. Mass transfer process was analyzed, and the changes in the polymer volume fractions during the membrane formation were simulated. In this model, the assumptions of isothermal process and negligible nonsolvent evaporation are rather critical since temperature changes due to evaporative cooling can be significant and simultaneous diffusion of solvent and nonsolvent, i.e. ternary diffusion, influences the membrane formation.

In this study, the formation of asymmetric porous structures by the dry-cast process was modeled, and the model was applied to cellulose acetate/acetone/water system. The primary purpose of this work is to clarify the relation between the membrane preparation conditions and the membrane structure based on both thermodynamic and kinetic aspects considered in the model. We attempt to show that appropriate formulation of the ternary diffusivities and accurate parameters used in these expressions form the heart of the membrane formation modeling. In particular, we will illustrate this point by comparing the model predictions resulting from different diffusion formulations with measurement of overall mass change as a function of time.

2. Theory

2.1. Kinetic model

The system shown schematically in Fig. 1 was chosen as a model system which can be simulated easily through laboratory scale experiments. This includes ternary polymer solution consisting of nonsolvent (1), solvent (2), and polymer (3) deposited on an impermeable substrate.

Initially, the polymer solution is assumed to have a uniform composition. At time $t = 0$, both the solvent and the nonsolvent begin evaporating into the gas phase. The gas phase next to the top side of the polymer solution is characterized by its temperature, T^G, the heat transfer coefficient, h^G, and the partial pressure of each volatile compound, P_{ib}^G, while the gas phase next to the bottom side of the substrate is distinguished by its temperature, T^g and the heat transfer coefficient, h^g, respectively. In our model formulation, the mass transfer is assumed to be one-dimensional and governed by Fickian diffusion; hence, the generalized Fick's law is used to describe the diffusive flux equations for the multicomponent system. Then, the species continuity equa-

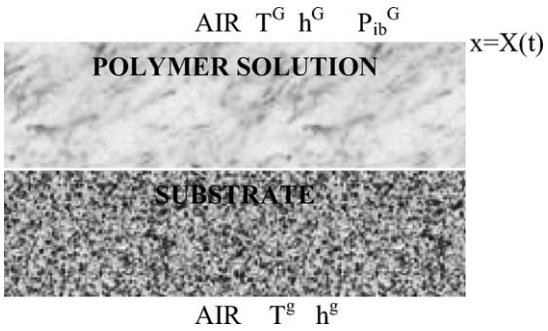

Fig. 1. Schematic of dry-casting process.

tion for each component based on volume average velocity as a reference frame is given by the equation

$$\frac{\partial \rho_i}{\partial t} = \frac{\partial}{\partial x}\left(\sum_{j=1}^{N-1} D_{ij}\frac{\partial \rho_j}{\partial x}\right) \tag{1}$$

In this equation, it is also assumed that the partial specific volume of all components are independent of the composition, i.e. there is no volume change on mixing. This assumption leads to the conclusion that the gradient of volume average velocity is zero. Based on this result, volume average velocity becomes zero everywhere in the solution since it is zero at the substrate–solution interface; hence, the convective term disappears in Eq. (1). During a typical membrane formation by dry-casting method, evaporation of the solvent and the nonsolvent have a significant evaporative cooling effect. In addition, membrane solution can be purposely heated by convective gas flow both from the top side of the solution and the bottom side of the substrate. These two effects result in a nonisothermal process and, therefore, induce coupled heat and mass transfer. In our formulation, temperature through the membrane forming solution and the substrate is uniform and the heat transfer is approximated by a lumped parameter approach. The time dependence of the temperature is then given by

$$\frac{\mathrm{d}T}{\mathrm{d}t} = -\left[\frac{h^{\mathrm{G}}(T-T^{\mathrm{G}}) + \sum_{i=1}^{N-1} k_i^{\mathrm{G}}\Delta\hat{H}_{\mathrm{v}i}(P_{ii}^{\mathrm{G}} - P_{i\mathrm{b}}^{\mathrm{G}}) + h^{\mathrm{g}}(T-T^{\mathrm{g}})}{\rho^{\mathrm{p}}\hat{C}_{\mathrm{p}}^{\mathrm{p}}X(t) + \rho^{\mathrm{s}}\hat{C}_{\mathrm{p}}^{\mathrm{s}}H}\right] \tag{2}$$

This approximation is fairly reasonable because the resistance to heat transfer in the gas phase is much greater than in the polymer solution or the substrate layer. In addition, the validity of this assumption was confirmed by the predictions of Shojaie et al. [15], which indicate flat temperature profiles at different times during membrane formation. Application of jump mass balance for each volatile species at the solution–gas-phase interface, $x = X(t)$, gives the following boundary condition.

$$x{=}X(t) \quad -\left(\sum_{j=1}^{N-1} D_{ij}\frac{\partial \rho_j}{\partial x}\right) - \rho_i\frac{\mathrm{d}X}{\mathrm{d}t} = k_i^{\mathrm{G}}(P_{ii}^{\mathrm{G}} - P_{i\mathrm{b}}^{\mathrm{G}}) \tag{3}$$

An expression for the time dependence of boundary position, $X(t)$, is derived from a jump mass balance for the polymer as follows:

$$\frac{\mathrm{d}X}{\mathrm{d}t} = -\left[\frac{\sum_{i=1}^{N-1} J_i^{\neq}\hat{V}_i}{1-\sum_{i=1}^{N-1}\rho_i\hat{V}_i}\right] \tag{4}$$

where diffusive flux of component i, $J_i^{\neq}$, with respect to volume average velocity is given by generalized Fick's law.

$$J_i^{\neq} = -\sum_{j=1}^{N-1} D_{ij}\frac{\partial \rho_j}{\partial x} \tag{5}$$

At the solution–substrate interface, $x = 0$, mass flux into the substrate is zero since the substrate is impermeable to the components in the polymer solution. Hence,

$$x = 0, \qquad \frac{\partial \rho_i}{\partial x} = 0 \tag{6}$$

Initially, the concentration of each solvent in the solution is uniform

$$\rho_i(0, x) = \rho_{i_0} \tag{7}$$

and the temperature and the thickness of the solution are known as

$$X(0) = L_0 \qquad T(0) = T_0 \tag{8}$$

2.2. Thermodynamic model

Theoretical treatment of membrane formation process requires combining the kinetics and thermodynamics of the system simultaneously. An appropriate thermodynamic model is necessary to construct ternary phase diagram, to formulate boundary conditions of the kinetic model and to calculate the chemical potential gradient of each component required in expressions of ternary diffusion coefficients. In this work, the Flory-Huggins thermodynamic theory with constant interaction parameters was used. According to this theory, the Gibbs free energy of mixing for multicomponent systems is given by the following equation.

$$\frac{\Delta G_{\mathrm{M}}}{RT} = \sum n_i \ln\phi_i + \sum \chi_{ij}\phi_i\phi_j \sum m_i n_i \quad \text{where} \quad i \neq j \tag{9}$$

Then, the chemical potential of each component was calculated from the first derivative of the expression given in Eq. (9) with respect to composition.

$$\frac{\Delta\mu_i}{RT} = \frac{\partial}{\partial n_i}\left(\frac{\Delta G_{\mathrm{M}}}{RT}\right)_{n_j, j\neq i} \tag{10}$$

2.3. Diffusion model

Theoretically, diffusion in a ternary system is described by four diffusion coefficients. The prediction of these diffusivities from the most general form of the multicomponent diffusion theory requires knowledge about friction coefficients, which provide a link between the self and mutual diffusion coefficients in the multicomponent mixtures [18,19]. Unfortunately, no experimental measurements are available on these coefficients or how they change as a function of composition. In this work, the friction-based diffusion model recently proposed by Alsoy and Duda [20] was used to predict multicomponent diffusivities. This model was derived from Bearman's statistical mechanial theory by assuming that the friction coefficients among all of the solute molecules are identically equal to zero. Then, ternary diffusivites are simply predicted from self diffusion and thermodynamic data as shown in Eqs. (11)–(14).

$$D_{11} = \rho_1(1-\rho_1\hat{V}_1)D_1\left(\frac{1}{RT}\frac{\partial\mu_1}{\partial\rho_1}\right) - \rho_1\rho_2\hat{V}_2D_2\left(\frac{1}{RT}\frac{\partial\mu_2}{\partial\rho_1}\right) \quad (11)$$

$$D_{12} = \rho_1(1-\rho_1\hat{V}_1)D_1\left(\frac{1}{RT}\frac{\partial\mu_1}{\partial\rho_2}\right) - \rho_1\rho_2\hat{V}_2D_2\left(\frac{1}{RT}\frac{\partial\mu_2}{\partial\rho_2}\right) \quad (12)$$

$$D_{21} = \rho_2(1-\rho_2\hat{V}_2)D_2\left(\frac{1}{RT}\frac{\partial\mu_2}{\partial\rho_1}\right) - \rho_1\rho_2\hat{V}_1D_1\left(\frac{1}{RT}\frac{\partial\mu_1}{\partial\rho_1}\right) \quad (13)$$

$$D_{22} = \rho_2(1-\rho_2\hat{V}_2)D_2\left(\frac{1}{RT}\frac{\partial\mu_2}{\partial\rho_2}\right) - \rho_1\rho_2\hat{V}_1D_1\left(\frac{1}{RT}\frac{\partial\mu_1}{\partial\rho_2}\right) \quad (14)$$

In these equations, the chemical potential gradients were evaluated from the Flory-Huggins thermodynamic theory, and the self diffusion coefficients were predicted from Vrentas-Duda free volume theory as follows [21,22].

$$D_1 = D_{o1}\exp\left(-\frac{\omega_1\hat{V}_1^* + \omega_2\hat{V}_2^*(\xi_{13}/\xi_{23}) + \omega_3\hat{V}_3^*\xi_{13}}{\hat{V}_{FH}/\gamma}\right) \quad (15)$$

$$D_2 = D_{o2}\exp\left(-\frac{\omega_1\hat{V}_1^*(\xi_{23}/\xi_{13}) + \omega_2\hat{V}_2^* + \omega_3\hat{V}_3^*\xi_{23}}{\hat{V}_{FH}/\gamma}\right) \quad (16)$$

$$\frac{\hat{V}_{FH}}{\gamma} = \frac{K_{11}}{\gamma}(K_{21}-T_{G1}+T)\omega_1 + \frac{K_{12}}{\gamma}(K_{22}-T_{G2}+T)\omega_2 + \frac{K_{13}}{\gamma}(K_{23}-T_{G3}+T)\omega_3 \quad (17)$$

3. Determination of model parameters

3.1. Free volume parameters

Free volume parameters of acetone and water were reported in the literature by Zielinski and Duda [23] and Hong [24]. However, neither free volume parameters nor WLF constants for cellulose acetate were reported in the literature. To determine these polymer specific parameters, K_{13}/γ, K_{23}–T_{G3}, the mixture parameter, $\hat{V}_3^*\xi_{23}$, the experimental self diffusion data of Anderson and Ullman [9] and Park [25] were fitted to Vrentas-Duda free volume theory. The product of critical polymer molar volume with the ratio of the jumping unit of water to that polymer, $\hat{V}_3^*\xi_{13}$, was obtained from $\hat{V}_3^*\xi_{13} = (\hat{V}_1^*M_1/M_{3j})$, in which jumping unit of polymer, M_{3j}, was calculated from the values determined for acetone as $M_{3j} = (\hat{V}_2^*M_2/\hat{V}_3^*\xi_{23})$. The free volume parameters and the Flory-Huggins interaction parameters obtained from Dabral et al. [26] for cellulose acetate/acetone, cellulose acetate/water and acetone/water systems are listed in Table 1. Among many model parameters required, accuracy of the free volume parameters significantly influence the predictions due to strong diffusional resistance controlling the dynamics of the membrane formation process. Diffusivity data, collected at a minimum of two temperatures, should be used if three of the free volume parameters in Table 1, E_i, K_{1i}/γ and K_{2I}–T_{gi} are regressed from the free volume theory. Otherwise, regressed parameters would not be reliable.

Table 1
Free volume and Flory-Huggins interaction parameters used in diffusivity correlations ($\chi_{12} = 1.3$)

Parameter		CA/acetone	CA/water
D_o	cm^2/s	3.6×10^{-4}	8.55×10^{-4}
K_{11}/γ	$cm^3/g\,K$	0.00186	0.00218
K_{12}/γ	$cm^3/g\,K$	0.000364	0.000364
$K_{21} - T_{G1}$	K	−53.33	−152.29
$K_{22} - T_{G2}$	K	−240	−240
$\hat{V}_1^*$	cm^3/g	0.943	1.071
$\xi_{13}\hat{V}_3^*$		0.715	0.252
χ		0.5	1.4

3.2. Heat and mass transfer coefficients

The heat and mass transfer coefficients for free convection conditions were determined using an empirical correlation developed for the horizontal cooled plates facing upward in the laminar regime [27]. The heat transfer coefficient was calculated from

$$\frac{hL_c}{k^G} = 0.27(Gr\cdot Pr)^{0.25} \quad (18)$$

and the mass transfer coefficient of each component was determined using the analogy between the heat and mass transfer [12].

$$\frac{k_iL_cy_{air,lm}\hat{V}_i^GP}{D_{i,G}} = 0.27(Gr\cdot Sc)^{0.25} \quad (19)$$

For the case of forced convection conditions, the heat and mass transfer coefficients were calculated by the correlations given in Eqs. (20) and (21) [28].

$$\frac{hL_c}{k^G} = 0.664Re^{0.5}Pr^{0.33} \quad (20)$$

$$\frac{k_iL_c\hat{V}_i^GP}{D_{i,G}} = 0.664Re^{0.5}Sc^{0.33} \quad (21)$$

3.3. Other parameters of the model

The saturated vapor pressure of acetone and water was calculated from Eq. (22) using constants given in Table 2 [29].

Table 2
The constants used in the calculation of vapor pressures of acetone and water

	Water	Acetone
A	−7.76451	−7.45514
B	1.45838	1.202
C	−2.7758	−2.43926
D	−1.23303	−3.35590
T_c (K)	647.3	508.1
P_c (bar)	221.2	47

Table 3
Physical properties of water, acetone, and cellulose acetate

	Water	Acetone	Cellulose acetate
Density (g/cm^3)	1.00	0.79	1.31
Molar volume (cm^3/mole)	18.0	73.92	30532
Heat of vaporization (J/g)	2444	552	

Table 4
Physical properties of polymer solution, substrate, and air

Glass support	
Density (g/cm^3)	2.5
Heat capacity (J/g K)	0.75
Polymer solution	
Heat capacity (J/g K)	2.5
Air	
Thermal conductivity (W/cm K)	2.55×10^{-4}

$$\ln\frac{P^{sat}}{P_c} = (1 - T_r)^{-1}[AT_r + BT_r^{1.5} + CT_r^3 + DT_r^6] \quad (22)$$

The physical properties, such as density, molar volume, heat of vaporization, and heat capacity, were obtained from various sources [15,28,30] and are listed in Tables 3 and 4.

4. Solution of the model equations

A robust algorithm was developed to construct the ternary phase diagram using the Flory-Huggins thermodynamic theory with constant interaction parameters. In this algorithm, calculation of tie lines was started from near the polymer–nonsolvent line and proceeded through the critical point. Due to the nature of polymer–nonsolvent interaction, the polymer concentration in the polymer lean phase approaches zero for most of the equilibrium points. Within this region, the routine sometimes assumes a negative value for the polymer volume fraction and can cause the program to stop because of the logarithmic operation in the chemical potential expression. To overcome this problem, the polymer volume fraction in the polymer lean phase was assumed to be zero. When the first tie line is calculated properly, the routine runs without any user input guess because the volume fraction of one component in one of the equilibrium phases was used as an initial guess in the calculation of the next tie line. All equations used in constructing the ternary phase diagram are nonlinear and were solved using an IMSL routine called DNEQNF. The details of the equations used in the algorithm can be found in the thesis of Ozbas [31]. Kinetic equations shown in Eqs. (1)–(8) are also highly nonlinear coupled differential equations and were solved using the finite difference approximation with a variable grid size. To facilitate numerical treatment of the moving boundary, a coordinate transformation was used, and, to reduce the stiffness of the equations, they were dimensionalized and updated according to the coordinate transformation [20,31].

5. Experimental

Cellulose acetate with a molecular weight of 50,000 and an acetyl content of 39.7% was purchased from Aldrich. Ninty nine percent pure acetone obtained from Merck was used as the solvent and distilled and deionized water was used as the nonsolvent. The CA was dried in an oven above 100 °C for several hours before used. No further purification was applied to the materials. Gravimetric measurements were carried out by casting the polymer solutions on 10 cm wide square glass substrates with the aid of a film applicator. After casting, the glass support was transferred to the microbalance within 15 s. In all experiments the lower side of the glass plate was insulated to prevent the heat transfer from the surface. The accumulation of the volatile components in the gas phase was not allowed by using an open chamber. As a result, the concentration in the gas phase was kept constant.

6. Results

The model shown in this work provides predictions of concentration of solvent, nonsolvent and polymer at any point in the solution, as well as the temperature and the thickness of the solution as a function of time. In the first part of this section, we have implemented model predictions to illustrate the effect of preparation conditions on the membrane morphology. In the second part, simulations were performed with different diffusion formalisms for three sets of experimental conditions in an attempt to validate the accuracy of the model and illustrate the effect of diffusion theory on the predictions.

6.1. Effect of concentration of nonsolvent in the casting solution

Morphological studies conducted on membranes obtained by phase inversion techniques have shown that composition of nonsolvent in the casting solution has a significant influence on the final membrane structure. To investigate this effect, volume fraction of cellulose acetate was kept constant, while the volume fraction of water was varied at 0.1,0.15, and 0.02. The simulations were denoted by Cases R1, R2,

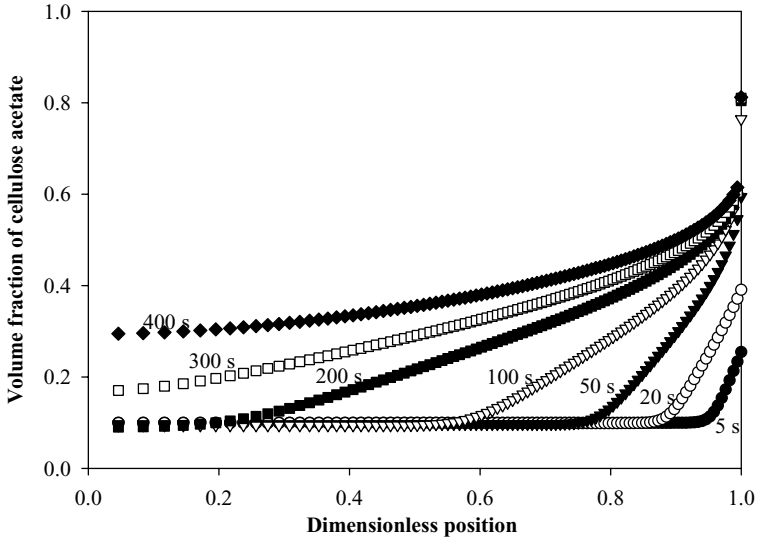

Fig. 2. Concentration profiles of cellulose acetate in the cellulose acetate/acetone/water system for Case R1.

R3, respectively. The parameters used for the simulations such as initial thickness of the solution, air temperature, heat, and mass transfer coefficients, and the relative humidity are given in Table 5. In order to illustrate the outputs resulting from the model, the predictions of concentration and temperature profiles, average concentrations, and thickness of the solution are shown in Figs. 2–6 for Case R1. The concentration profiles of cellulose acetate, water, and acetone are expressed in terms of volume fraction. Figs. 2–4 indicate that, at the initial stages of membrane formation, the rate of evaporation of acetone is very fast compared to that of water. This leads to very sharp concentration gradients of acetone especially at the solution–air interface ($\eta = 1$); thus, the concentration of CA increases rapidly at that surface. Average volume fractions of three components presented in Fig. 5 show the interesting change in water concentration during the membrane formation. As acetone evaporates, the volume of the solution decreases, and the concentration of water increases to a maximum and begins to decrease after 400 s. Due to both water and acetone evaporation, the initial casting solution undergoes shrinkage. This effect is clearly seen in Fig. 6, which shows an asymptotic decrease in thickness of the solution from 200 μm to about 53 μm in 400 s. Another important prediction from the model is the temperature of the solution and the substrate as a function of time. Most of the previous studies of evaporative casting of polymer films have ignored the evaporative cooling effect on mass transfer rates. Shojaie et al. [15,16] incorporated the effect of evaporative cooling by solving the unsteady state heat transfer equation, and predicted that temperature profiles throughout the membrane formation are flat. In our model, a single uniform temperature for the polymer film

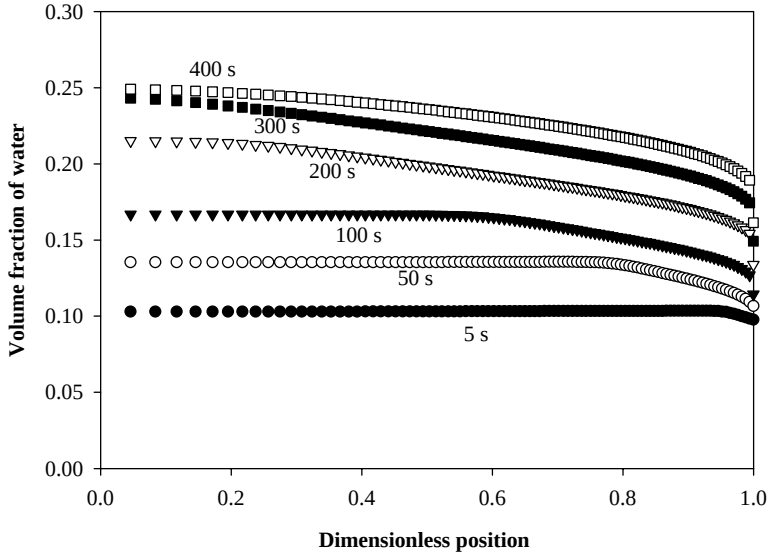

Fig. 3. Concentration profiles of water in the cellulose acetate/acetone/water system for Case R1.

Table 5
Input parameters used in simulations

Code of simulated cases	Volume fractions			Initial solution temperature (°C)	Temperature of air (°C)	Initial casting thickness (μ)	Relative humidity (%)	Mode of convection	Mass transfer coefficients (sec/cm)		Heat transfer coefficients (W/cm^2 K)	
	Water	Acetone	CA						Water	Acetone	Film side	Substrate side
R1	0.1	0.8	0.1	23	24	200	0	Free	1.2×10^{-10}	5.5×10^{-10}	2.2×10^{-4}	Insulated
R2	0.15	0.75	0.1	23	24	200	0	Free	1.3×10^{-10}	5.1×10^{-10}	2.2×10^{-4}	Insulated
R3	0.02	0.88	0.1	23	24	200	0	Free	9.2×10^{-11}	6.2×10^{-10}	2.2×10^{-4}	Insulated
R4	0.1	0.8	0.1	23	24	120	0	Free	1.2×10^{-10}	5.5×10^{-10}	2.2×10^{-4}	Insulated
R5	0.1	0.8	0.1	23	24	120	50	Free	6.4×10^{-11}	5.5×10^{-10}	2.2×10^{-4}	Insulated
R6	0.1	0.8	0.1	23	24	120	0	Forced	5.9×10^{-10}	1.2×10^{-09}	8.4×10^{-4}	Insulated
R7	0.05	0.85	0.1	23	24	140	50	Free	9.7×10^{-11}	5.9×10^{-10}	2.5×10^{-4}	Insulated
R8	0.15	0.80	0.05	23	24	166	60	Free	8.8×10^{-11}	4.9×10^{-10}	2.2×10^{-4}	Insulated

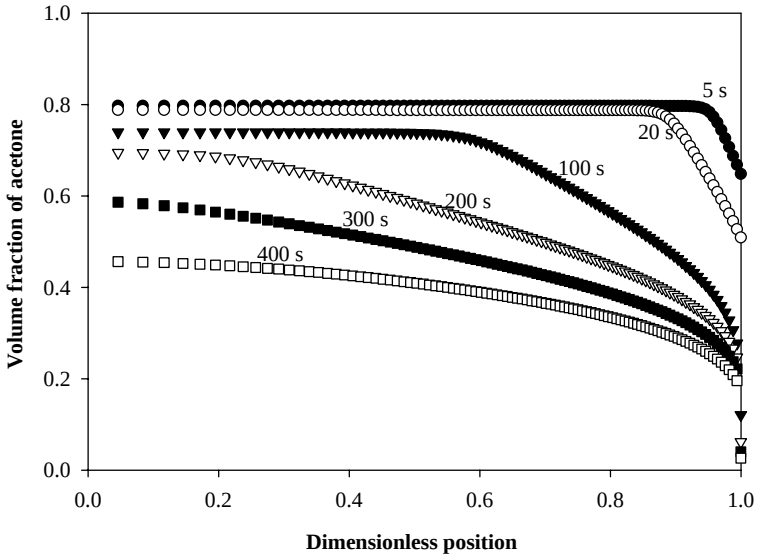

Fig. 4. Concentration profiles of acetone in the cellulose acetate/acetone/water system for Case R1.

and substrate layer are assumed since the gas-phase convective resistance to heat transfer is much greater than the conductive resistance in the polymer and substrate layers. This approach reduces the number of equations and promotes the numerical solution without losing the accurate representation of physical phenomena. The temperature profile with respect to time for Case R1, also shown in Fig. 6, indicates that evaporative cooling is significant due to fast evaporation of acetone. The casting solution is initally at 23 °C and, in 400 s, temperature decreases about 9 °C. This cooling influences the dry-cast process significantly due to apparent temperature dependence of both diffusivities and vapor pressures of the solvent and nonsolvent.

Model predictions provide information on the structure of the membrane when composition paths as a function of time are superimposed on the ternary phase diagram and polymer concentration versus position at the moment of precipitation are plotted. Composition paths on the ternary phase diagram enable the assessment of whether a phase separation occurs and allow prediction of the inception time and the duration of the phase separation. The polymer distribution at the moment of precipitation provides a rough thickness of the high polymer concentration region near the interface and the pore distribution of the sublayer structure.

In Fig. 7, concentration paths in time for the substrate/solution and solution /air interface are shown. One can observe from this Fig. that the concentration paths of these two interfaces (the solution/air and the solution/substrate interfaces) cross the binodal curve at markedly different times (424 and 383 s, respectively). Also, the free surface

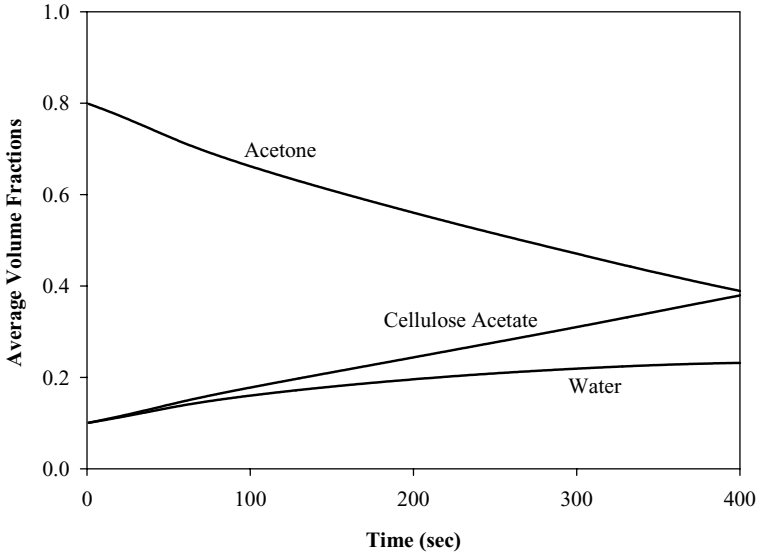

Fig. 5. Average concentration of water, acetone, and cellulose acetate during the membrane formation for Case R1.

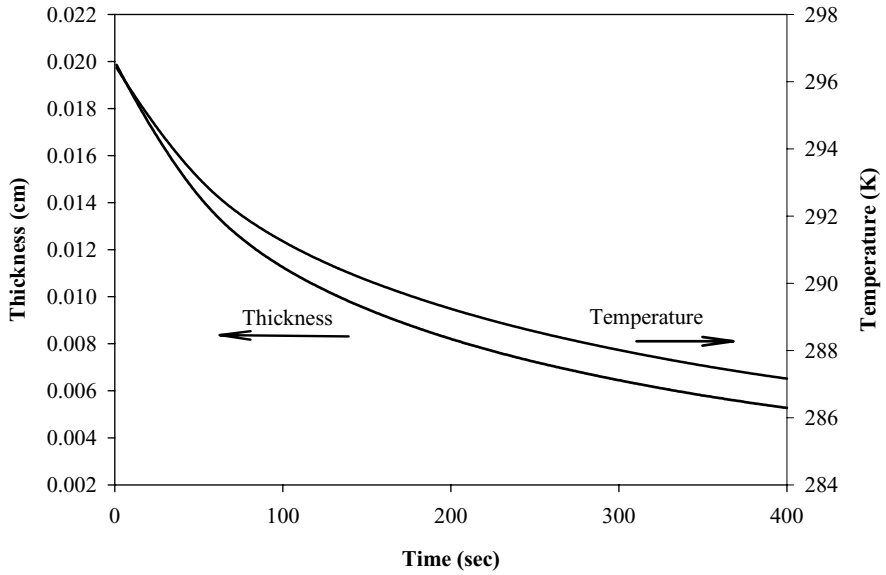

Fig. 6. Thickness and temperature change of the polymer solution as a function of time for Case R1.

enters the phase envelope at a polymer volume fraction of 0.82, while the substrate-solution interface enters with a volume fraction of 0.28. Based on these two observations, one might expect that the casting conditions represented by Case R1 will produce a porous asymmetric membrane in which the upper surface is much denser than the lower surface. The effect of increasing the volume fraction of water in the casting solution is shown in Fig. 8. The composition paths in this Fig. correspond to Case R2 in Table 5 in which the casting solution consists of 15% water, 75% acetone and 10% CA. The increase in nonsolvent concentration in the casting solution leads to earlier phase separation; the solution–air and the substrate–solution interfaces reach the phase boundary at 365 and 340 s, respectively. In addition,

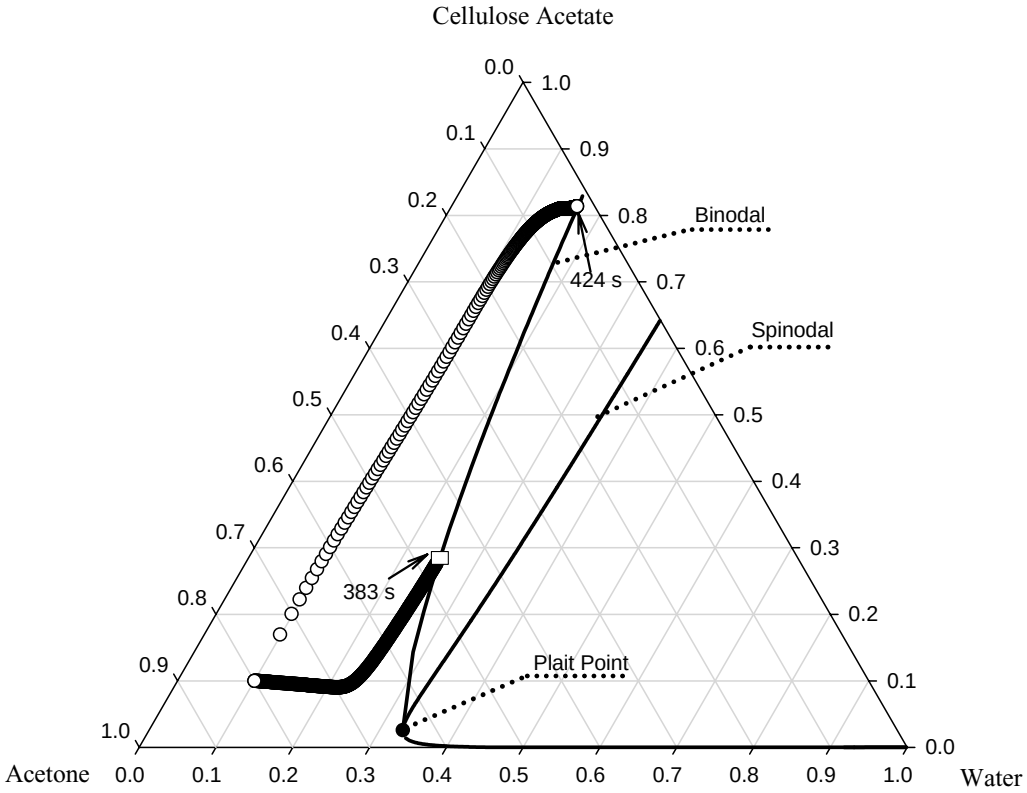

Fig. 7. Concentration paths of water, acetone and cellulose acetate for Case R1 ((○) solution/air interface, (□) solution/substrate interface).

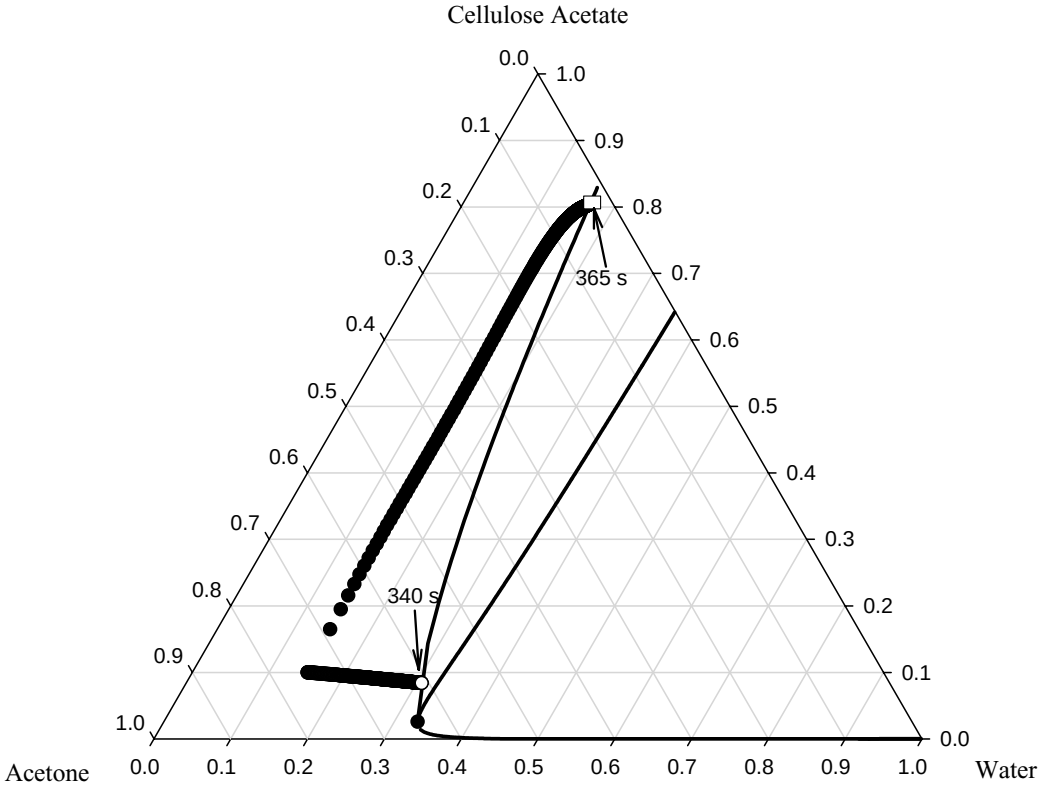

Fig. 8. Concentration paths of water, acetone and cellulose acetate for Case R2 ((○) solution/substrate interface, (□) solution/air interface).

the difference in concentration of CA at these two interfaces becomes larger. To obtain more explicit information on the structure of the membranes formed from two different casting compositions, the polymer concentration profiles of Cases R1 and R2, both corresponding to precipitation time, were plotted as shown in Fig. 9. Asymmetric membranes are usually described in terms of a skin thickness. We have defined the surface skin thickness as the distance between the free surface and the point in which the concentration of polymer decreases by 30%. According to this qualitative criteria, the percentage of dense skin layer decreases from 2.92 to 1.38% as volume fraction of water in the initial casting solution was increased from 10 to 15%. Additionally, Fig. 9 shows that with increased nonsolvent concentration,

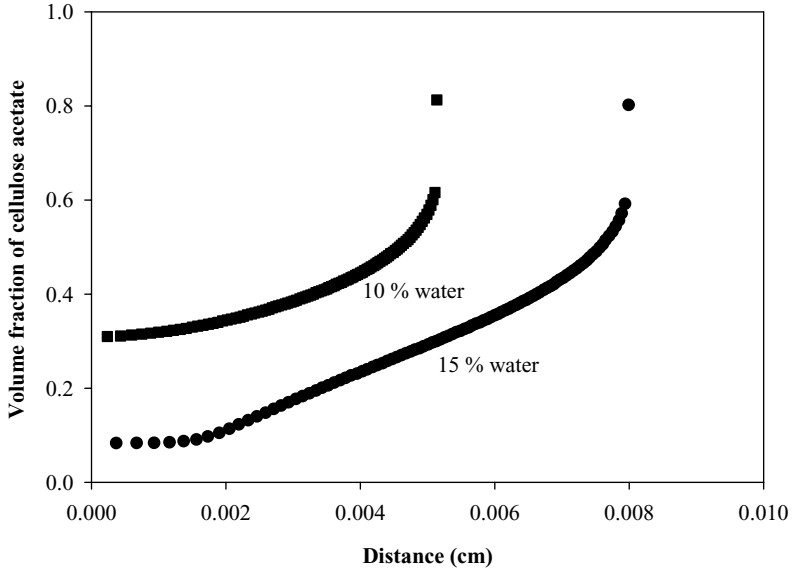

Fig. 9. Polymer concentration profiles in the membrane for Cases R1 and R2 at the moment of precipitation.

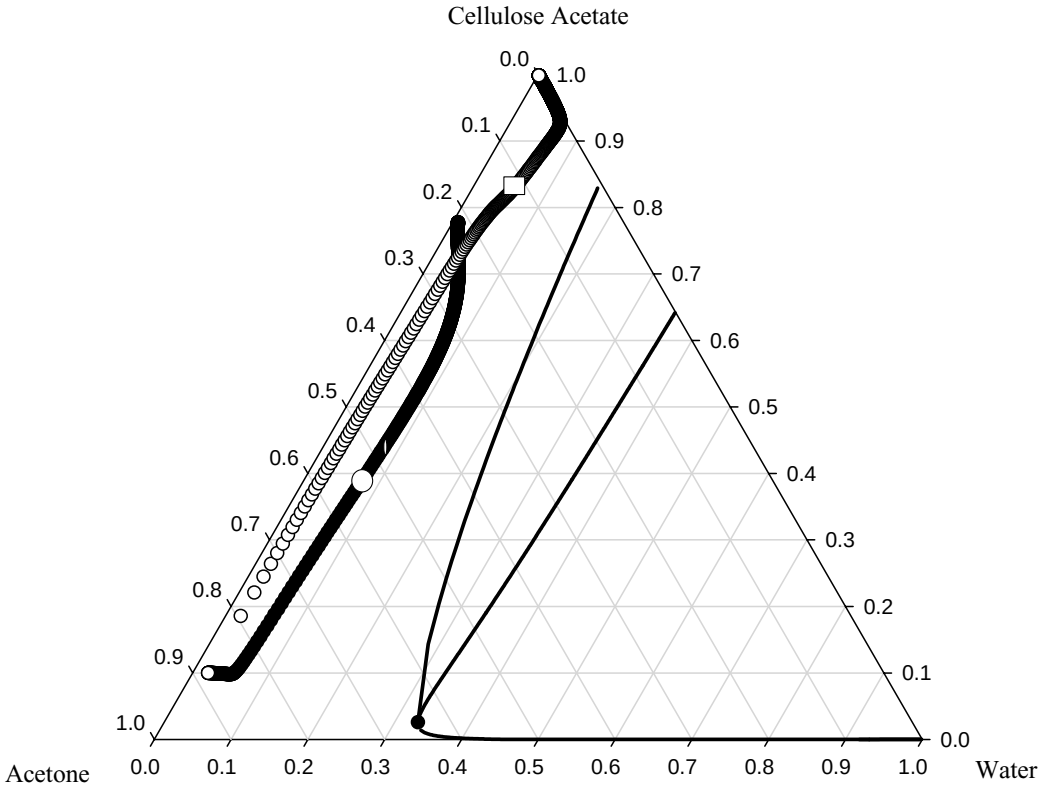

Fig. 10. Concentration paths of water, acetone, and cellulose acetate for Case R3 ((○) solution/substrate interface, (□) solution/air interface).

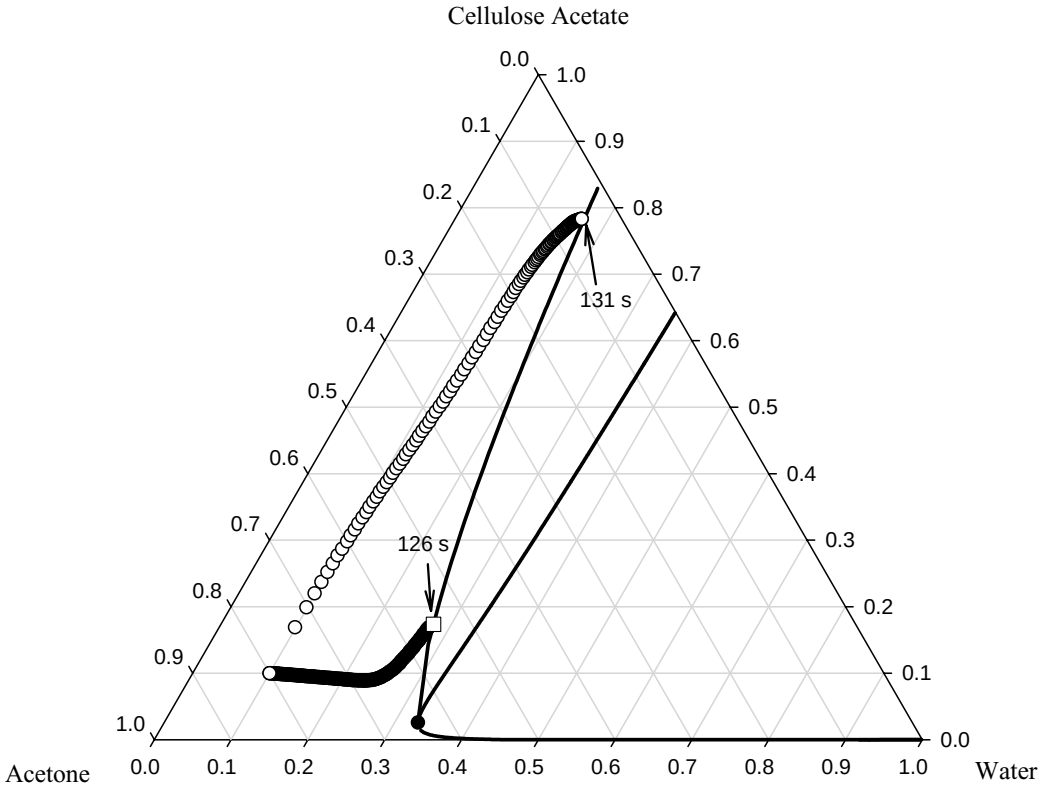

Fig. 11. Concentration paths of water, acetone, and cellulose acetate for Case R4 ((○) solution/air interface, (□) solution/substrate interface).

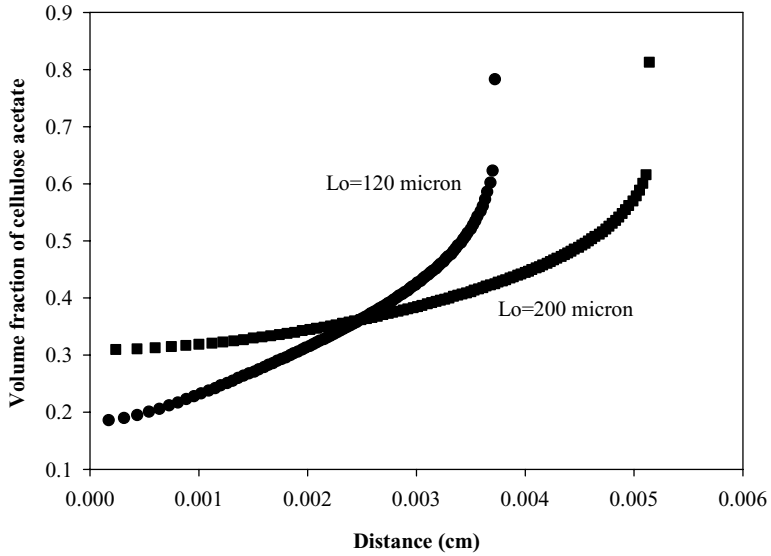

Fig. 12. Polymer concentration profiles in the membrane for Cases R1 and R4 at the moment of precipitation.

the film shrinkage rate is decreased and the formation of much more graded pore sublayer structure having higher porosity is favored due to lower polymer concentration in that region. Then, the predictions in Fig. 9 imply that the membrane structure becomes more asymmetric by increasing the nonsolvent concentration in the casting solution. In order to determine whether there is an optimum concentration of nonsolvent below which no porous structure is obtained, volume fraction of water in the initial casting solution was reduced to 0.02 while volume fraction of polymer was kept at 0.1, corresponding to Case R3 in Table 5. The composition paths on the phase diagram shown in Fig. 10 illustrate that neither the air side nor the support side enter the two-phase region. The prediction implies that, when initial

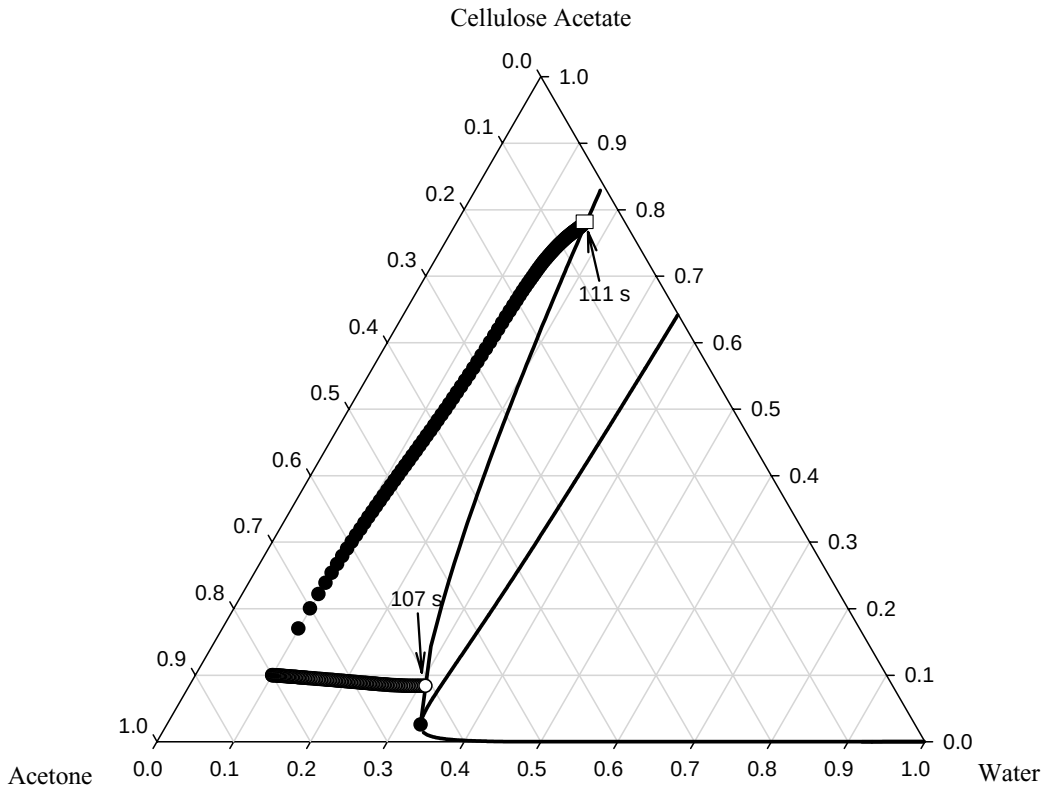

Fig. 13. Concentration paths of water, acetone, and cellulose acetate for Case R5 ((○) solution/substrate interface, (□) solution/air interface). Prediction was performed through the insertion of full diffusion model [20].

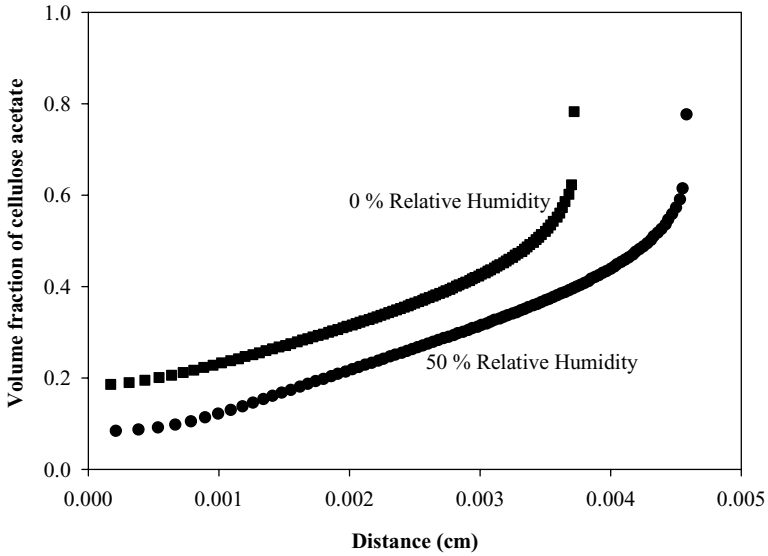

Fig. 14. Polymer concentration profiles in the membrane for Cases R4 and R5 at the moment of precipitation.

nonsolvent concentration in the casting solution is low, the phase separation may not take place and a dense nonporous film may be obtained rather than a porous membrane.

6.2. Effect of initial thickness of the casting solution

The effect of initial thickness of the casting solution on the membrane formation process is shown in Fig. 11. Simulation conditions are denoted by Case R4 and are identical to those of Case R1, except that the initial film thickness is 120 μm. Comparing composition paths plotted on the phase diagrams in Figs. 7 and 11 indicates that decreasing the initial film thickness leads to faster phase separation since, in this case, total mass of acetone is less than that of case R1. In addition, the difference in polymer concentrations at the top and bottom interfaces is larger. The polymer distribu-

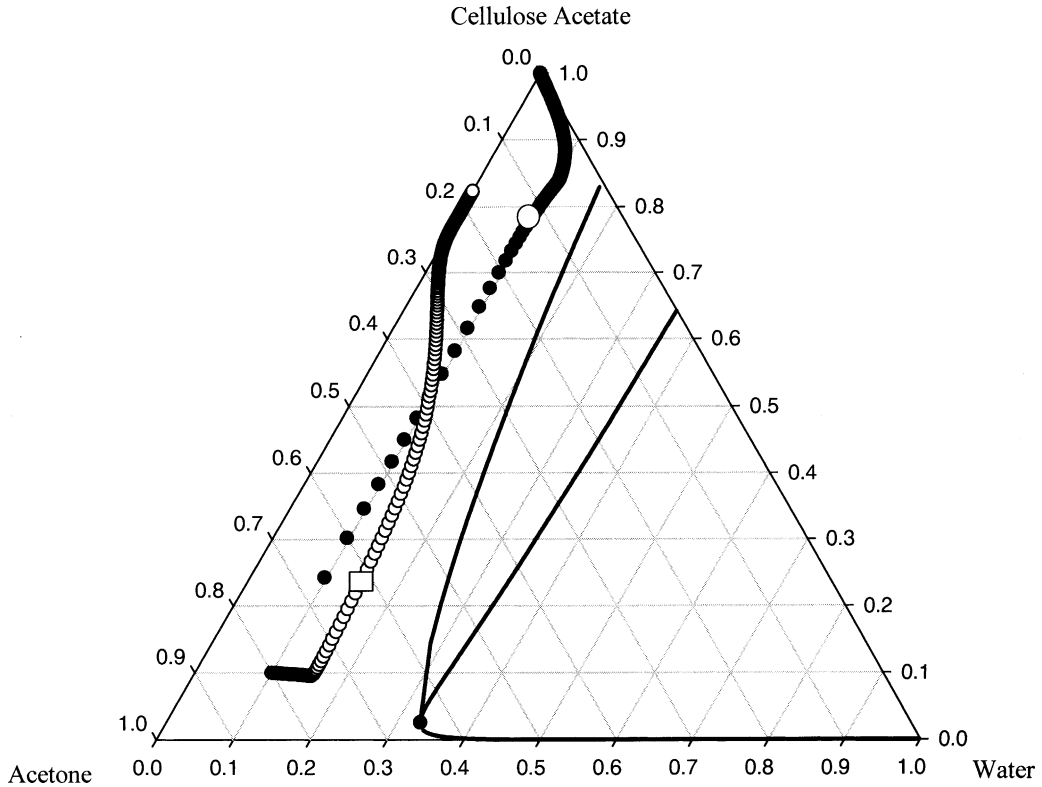

Fig. 15. Concentration paths of water, acetone, and cellulose acetate for Case R6 ((○) solution/air interface, (□) solution/substrate interface).

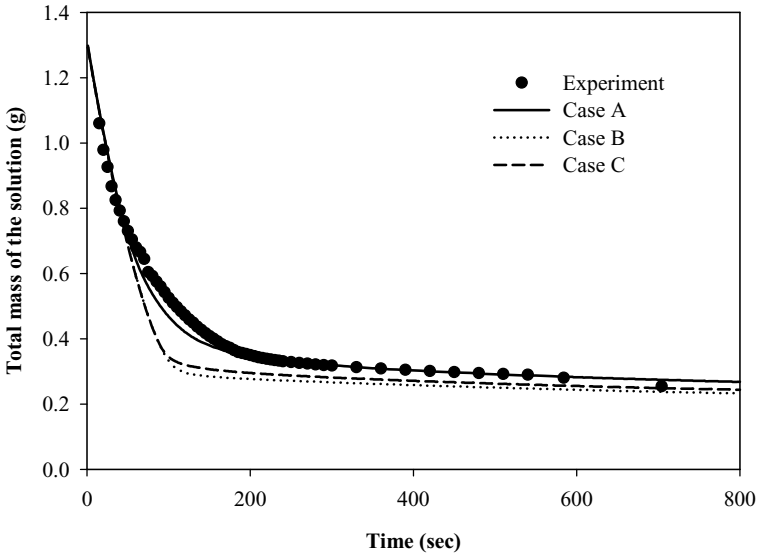

Fig. 16. Experimental and simulation results for total solution mass as a function of time for Case R7. Predictions were performed through the insertion of three different diffusion formalims into the model.

tions for both cases, shown in Fig. 12 indicate that decreasing the initial thickness of the casting solution leads to the formation of a thicker skin layer and a more graded pore sublayer structure with higher porosity towards the bottom of the membrane. The percentage of dense skin layer was found to increase from 2.92 to 4.03% as the initial thickness of the solution was decreased from 200 to 120 μm.

6.3. Effect of relative humidity

To investigate the effect of relative humidity on the membrane structure, simulations were performed, denoted by Case R5, in which all conditions are identical to those of Case R4 except that the relative humidity of air was increased to 50%. Comparison of the composition paths in Figs. 11 and 13 and the polymer distributions in Fig. 14 indicate that increasing the relative humidity of air affects the formation process in two ways. First, the solution/air and substrate/solution interfaces enter into the phase diagram more rapidly and not at the same time. As the relative humidity of air increases, the driving force for the evaporation of water decreases causing more residual water trapped in the solution, and thus, more rapid phase separation. Second, increasing the relative humidity will lead to a more graded and porous membrane structure with a thinner skin layer. The percentages of dense skin layers were determined as 3.28 and 4.03%, when relative humidity of air is 50 and 0%, respectively.

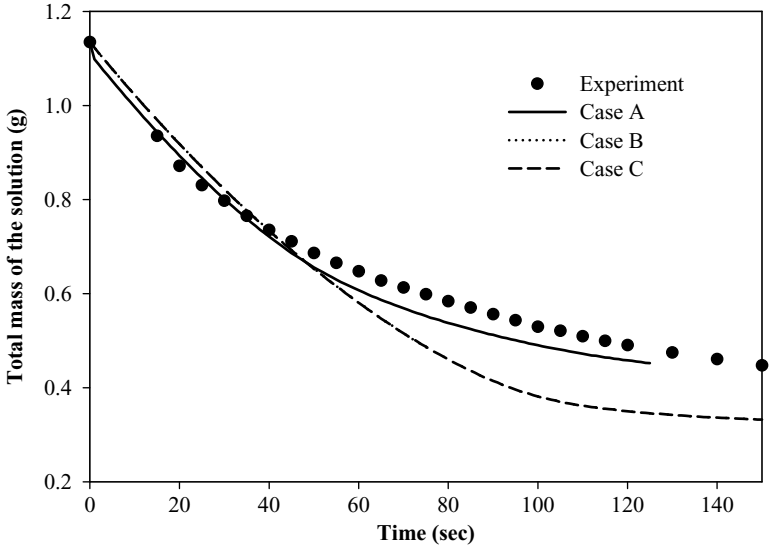

Fig. 17. Experimental and simulation results for total solution mass as a function of time for Case R5. Predictions were performed through the insertion of three different diffusion formalims into the model.

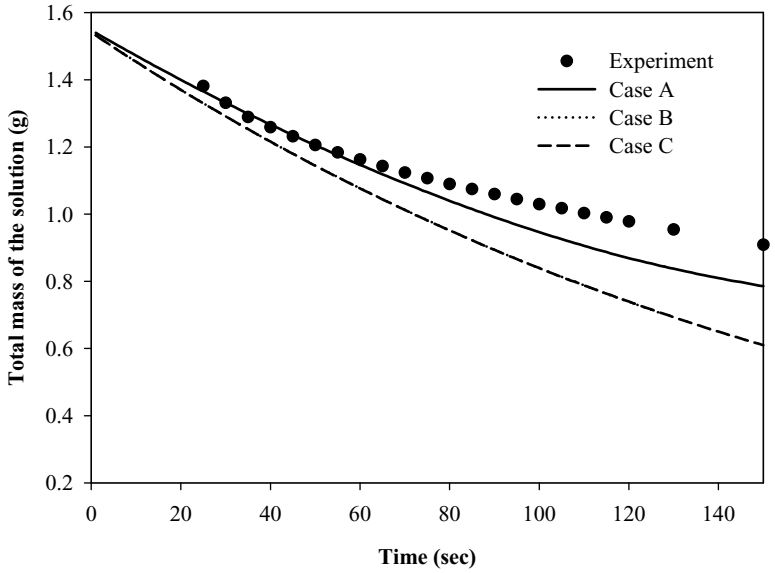

Fig. 18. Experimental and simulation results for total solution mass as a function of time for Case R8. Predictions were performed through the insertion of three different diffusion formalims into the model.

6.4. Effect of evaporation condition

In all cases reported so far, the heat and mass transfer from the cast polymer solution to the gas phase were controlled by free convection process. To investigate the effect of evaporation condition on the membrane structure, a simulation was performed, denoted by Case R6, in which the velocity of air was set as 50 cm/s while all other parameters were kept the same as those reported for Case R4. Comparison of composition paths for these two cases, shown in Figs. 11

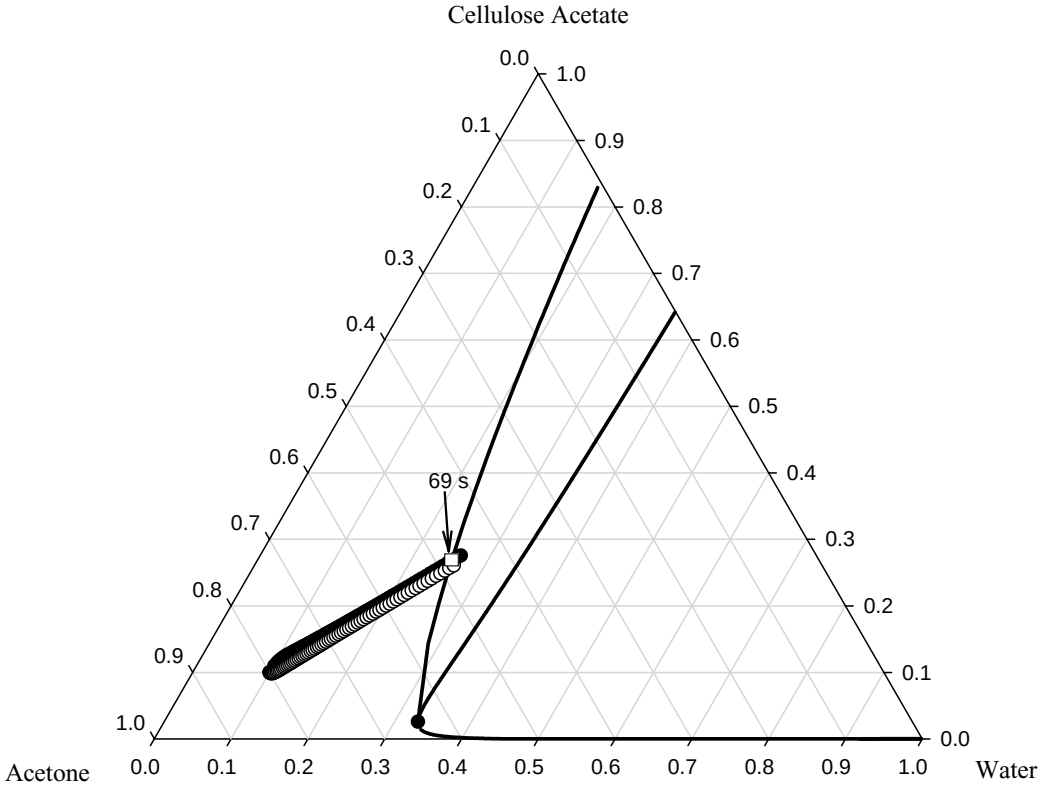

Fig. 19. Concentration paths of water, acetone and cellulose acetate for Case R5. ((○) solution/substrate interface, (●) solution/air interface). Prediction was performed through the insertion of diffusion model using only the principal diffusion coefficients (i.e., the cross diffusion coefficients were set equal to zero).

and 15, points out that with increasing air velocity, phase separation is completely suppressed and a uniformly dense coating devoid of substantial microstructure will result.

6.5. Test of predictive ability of the model and effect of diffusion formalism

The measurement of variables in real time for the membrane formation is very difficult. Such analysis requires highly sophisticated techniques. Shoajaie et al. [16] and Greenberg et al. [32] used the infrared thermography technique, which provides both gravimetric and thermal information. In addition, the onset and duration of the phase separation were determined by light intensity measurements. In this work, the validity of the model was confirmed using the measurement of total evaporation rate by monitoring the overall mass change as a function of time. Three sets of gravimetric measurements were carried out. The experimental conditions and other input data used in the simulations are represented by Cases R5, R7 and R8. In each case, simulations have been conducted for three alternative approximations of the ternary diffusion coefficients. In Case A, all four ternary diffusion coefficients were used; however, in Case B, cross diffusion coefficients (D_{12} and D_{21}) were set to zero. Case C represents the commonly used simplest approximation, where the cross diffusion coefficients are equal to zero and the main diffusion coefficients (D_{11} and D_{22}) are predicted by the corresponding self diffusion coefficients without considering the thermodynamic factor. Experimental evaporation data for the cellulose acetate/acetone/water system accompanied by corresponding predictions from the model are shown in Figs. 16–18. On the basis of the results it can be noted that predictions for all cases are essentially equivalent at the initial stages of evaporation since mass transfer is controlled by external conditions. At later stages of membrane formation, the predictions from the Case A model are noticeably better than those from the Case B and the Case C diffusion models. These results indicate that cross diffusion coefficients are not negligible and the thermodynamic factor is significant, both of which influence the predictions of total mass of the solution. We have calculated the sum of the square of the difference between the experimental points and the model predictions from Case A as 0.061, 0.026, and 0.097, respectively for each experimental data set shown in Figs. 16–18. According to these values, the full diffusion model, i.e. Case A, produces the best result for the second experimental data sets and the worst result for the third experimental data sets. However, it must be noted that the dry cast model shown in this study does not contain any adjustable parameters. The predictions are based only on conservation laws, solution thermodynamics, and measured and correlated values of the relevant physical and transport properties. In light of this fact, and considering reliability of numerous number of parameters required

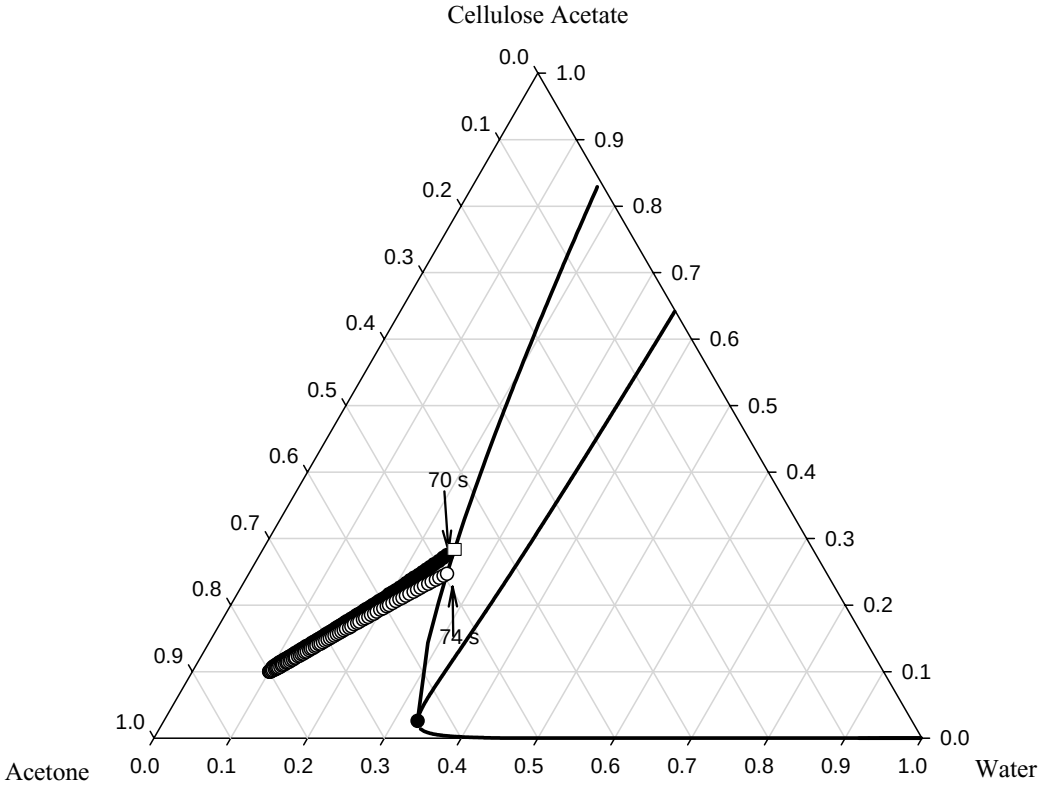

Fig. 20. Concentration paths of water, acetone, and cellulose acetate for Case R5. ((○) solution/substrate interface, (□) solution/air interface). Prediction was performed through the insertion of diffusion model in which the cross diffusion coefficients were set equal to zero and the principal diffusion coefficients were estimated by corresponding self diffusion coefficients).

for the model, the slight deviation between the experimental data and the predictions in Case R8 is quite reasonable.

The effect of diffusion formalism on the prediction of structure formation was investigated by comparing the composition paths on the phase diagram corresponding to the experimental conditions represented by Case R5. As shown in Figs. 19 and 20, composition paths obtained from simplified diffusion models (Cases B and C) are similar. However, they differ in two ways from the corresponding paths in Fig. 13 predicted through insertion of the full diffusion model (Case A). First, the interfaces enter the phase envelope at different times. In Case A, the binodal line is crossed around 110 s while in Cases B and C, composition paths enter into the two phase region around 70 s. Second, the differences in polymer compositions of the two interfaces when they cross the binodal curve are not the same. In fact, the predictions resulting from Cases B and C suggest that final membrane structure will be porous and symmetric. However, the counterpart model predictions generated from the full diffusion model (Case A) imply that membrane structure will be highly asymmetric and porous since compositions of the polymer at the solution/air and the substrate/solution interfaces are markedly different. The striking differences in the prediction of structure formation from three different diffusion formalisms clearly point out the need for an accurate formulation of diffusion theory in membrane formation modeling.

7. Conclusions

We have implemented a drying model to predict the formation of asymmetric membranes by dry-casting method. The model is fully predictive, i.e. does not contain any adjustable parameters. It is based on fundamental conservation laws, thus, can be applied to any membrane forming system. The predictive ability of the model was evaluated by comparing the experimentally measured total weight of the solution with the model predictions. While the agreement between the model predictions and two sets of experimental data is good, the model slightly underpredicts the data for a case in which polymer was dilute in solution. Based on these comparisons, we suggest that the model performs adequately well and can be used as a practical tool for optimizing membrane production by the dry-casting process. Obviously, this analysis is only a first step toward an accurate description of multicomponent diffusion in membrane formation modeling. More experimental results, such as morphological studies or light intensity data are needed to evaluate the model.

The model predictions indicated that concentration of water (nonsolvent) in the initial casting solution and evaporation conditions have substantial influences on the structure of the membrane. Without altering polymer, solvent, or nonsolvent, it is possible to vary the structure from dense to porous asymmetric by either increasing the nonsolvent composition in the solution or decreasing the air velocity during evaporation. We also found that diffusion formalism plays an important role in capturing the accurate structure of the membrane. This work clearly confirms that accurate formulation and prediction of ternary diffusivities forms the basis and heart of the membrane formation modeling. Simplifications in the diffusion theory such as the elimination of cross diffusion coefficients (as is common practice) lead to incorrect conclusions about the structure of the membrane that will be obtained from a particular casting condition. The model can also be used to study the influence of initial solution temperature or air temperature on the phase inversion dynamics. Increasing the air temperature and the initial solution temperature cause more rapid phase separation since both diffusion coefficients and the activities of the solvent and nonsolvent, thus their evaporation rates, increase. With a decreased solubility between solvent and nonsolvent, a decreased miscibility gap and a more rapid phase separation are predicted from the thermodynamic and the kinetic models, respectively.

Nomenclature

$\hat{C}_p$	specific heat capacity (J/g K)
D_{ij}	cross diffusion coefficient (cm^2/s)
D_{ii}	main diffusion coefficient (cm^2/s)
D_i	self diffusion coefficient of component i (cm^2/s)
$D_{i,G}$	diffusivity of component i in the gas phase (cm^2/s)
D_{oi}	preexponential factor of component i (cm^2/s)
Gr	Grashof number for mass transfer
G_M	Gibbs free energy of mixing
h	heat transfer coefficient (W/cm^2 K)
H	thickness of the substrate (cm)
k_i	mass transfer coefficient of component i (s/cm)
K_{1i}/γ	free volume parameter of component i (cm^3/g K)
K_{2i}	free volume parameter of component i (K)
L_0	initial thickness of the polymer solution (cm)
L_c	characteristic length of the substrate (cm)
n_i	number of moles of component i (mole)
P_{ii}	partial pressure of component i at the interface (g/cm s^2)
P_{ib}	partial pressure of component i in the gas phase (g/cm s^2)
Pr	Prandtl number
P	total pressure (g/cm s^2)
P_c	critical pressure (g/cm s^2)
P^{sat}	vapor pressure (g/cm s^2)
Re	Reynolds number
R	gas constant (cm^3 atm/mole K)
Sc	Schmidt number

T	temperature (K)
T_0	initial temperature of the substrate and polymer film (K)
T_{gi}	glass transtion temperature of component i (K)
T_r	reduced temperature
t	time (sec)
$X(t)$	thickness of the polymer solution as a function of time (cm)
x	position (cm)
$\hat{V}_i^*$	specific critical hole free volume of component i required for a jump (cm^3/g)
$\hat{V}_i$	partial specific volume of component i (cm^3/g)
$y_{air,lm}$	log mean mole fraction difference of component i in the gas phase

Greek letters

χ_{ij}	Flory-Huggins interaction parameter between component i and j
η	dimensionless distance
μ_i	chemical potential of component i (cm^3 atm/mole. K)
ξ_{ij}	ratio of critical molar volume of jumping unit of component i to that of component j
ω_i	weight fraction of component i
ϕ_i	volume fraction of component i
$\Delta\hat{H}_{vi}$	heat of vaporization of component i (J/g)
ρ_{i_0}	initial mass density of component i (g/cm^3)
ρ_i	mass density of component i (g/cm^3)

Superscripts

p	polymer solution
s	substrate
G	gas

References

[1] W.J. Koros, G.K. Fleming, Membrane-based gas separation, J. Membr. Sci. 83 (1993) 1.

[2] P. vandeWitte, P.J. Dijkstra, J.W.A. vandenBerg, J. Feijen, Phase separation processes in polymer solutions in relation to membrane formation, J. Membr. Sci. 117 (1996) 1.

[3] P. Radovanovic, S.W. Thiel, S.T. Hwang, Formation of asymmetric polysulfone membranes by immersion precipitation. 2. The effects of casting solution and gelation bath compositions on membrane-structure snd skin formation, J. Membr. Sci. 65 (1992) 231.

[4] I.M. Wienk, R.M. Boom, M.A.M. Beerlage, A.M.W. Bulte, C.A. Smolders, H. Strathmann, Recent advances in the formation of phase inversion membranes made from amorphous or semi-crystalline polymers, J. Membr. Sci. 113 (1996) 361.

[5] H.C. Park, Y.P. Kim, H.Y. Kim, Y.S. Kang, Membrane formation by water vapor induced phase inversion, J. Membr. Sci. 156 (1999) 169.

[6] A.M.W. Bulte, B. Folkers, M.H.V. Mulder, C.A. Smolders, Membranes of semicrystalline aliphatic polyamide nylon-4,6—formation by diffusion-induced phase-separation, J. Appl. Polym. Sci. 50 (1993) 13.

[7] D.R. Lloyd, K.E. Kinzer, H.S. Tseng, Microporous membrane formation via thermally induced phase-separation. 1. Solid liquid-phase separation, J. Membr. Sci. 52 (1990) 239.

[8] I. Pinnau, W.J. Koros, Structures and gas separation properties of asymmetric polysulfone membranes made by dry, wet, and dry wet phase inversion, J. Appl. Polym. Sci. 43 (1991) 1491.

[9] J.E. Anderson, R. Ullman, Mathematical analysis of factors influencing the skin thickness of asymmetric reverse osmosis membranes, J. Appl. Phys. 44 (1973) 4303.

[10] C. Castellari, S. Ottani, Preparation of reverse osmosis membranes. A numerical analysis of asymmetric membrane formation by solvent evaporation from cellulose acetate casting solutions, J. Membr. Sci. 9 (1981) 29.

[11] W.B. Krantz, R.J. Ray, R.L. Sani, K.J. Gleason, Theoretical study of the transport processes occurring during the evaporation step in asymmetric membrane casting, J. Membr. Sci. 29 (1986) 11.

[12] C.S. Tsay, A.J. McHugh, Mass transfer dynamics of the evaporation step in membrane formation by phase inversion, J. Membr. Sci. 64 (1991) 81.

[13] S.B. Tantekin-Ersolmaz, The Evaporation Step in Asymmetric Membrane Formation: Modeling, Gravimetric/Inframetric, and Morphology Studies, PhD Dissertation, University of Colorado, Boulder, CO, 1990.

[14] S.S. Shojaie, W.B. Krantz, A.R. Greenberg, Development and validation of a model for the formation of evaporatively cast polymeric films, J. Mater. Process Manuf. Sci. 1 (1992) 181.

[15] S.S. Shojaie, W.B. Krantz, A.R. Greenberg, Dense polymer film and membrane formation via the dry cast process. Part I. Model development, J. Membr. Sci. 94 (1994a) 255.

[16] S.S. Shojaie, W.B. Krantz, A.R. Greenberg, Dense polymer film and membrane formation via the dry cast process. Part II. Model validation and morphological studies, J. Membr. Sci. 94 (1994) 281.

[17] H. Matsuyama, M. Teramoto, T. Uesaka, Membrane formation and structure development by dry cast process, J. Membr. Sci. 135 (1997) 271.

[18] R.J. Bearman, On the molecular basis of some current theories of diffusion, J. Phys. Chem. 65 (1961) 1961.

[19] J.S. Vrentas, J.L. Duda, A.C. Hou, Enhancement of impurity removal from polymer films, J. Appl. Polym. Sci. 30 (1985) 4499.

[20] S. Alsoy, J.L. Duda, Modeling of multicomponent drying of polymer films, AIChE J. 45 (1999) 896.

[21] R.D. Ferguson, E. Von Meerwall, Free volume interpretation of self diffusion in ternary solutions: n-Paraffin-Hexafluoro-benzene-cis-4-Polybutadiene, J. Poly. Sci. B. Polym. Phys. 18 (1980) 1285.

[22] J.S. Vrentas, J.L. Duda, H.C. Ling, Self-diffusion in polymer solvent systems, J. Polym. Sci. 22 (1984) 459.

[23] J.M. Zielinski, J.L. Duda, Predicting polymer/solvent diffusion coefficients using free-volume theory, AIChE J. 38 (1992) 405.

[24] S. Hong, Prediction of polymer/solvent solution behavior using free volume theory, Ind. Eng. Chem. Res. 34 (1995) 2536.

[25] G.S. Park, Radioactive studies of diffusion in polymer systems.3. Sorption and self-diffusion in acetone + cellulose acetate system, Trans. Faraday Soc. 57 (1961) 2314.

[26] M. Dabral, L.F. Francis, L.E. Scriven, in: Proceedings of the Ninth International Coating Science and Technology Symposium Final Program and Extended Abstracts on Structure Evolution in Asymmetric Polymer Coatings, Newark, Delaware, 1998.

[27] W.H. McAdams, Heat Transmission, third ed., McGraw-Hill, New York, 1954.
[28] F.P. Incropera, D.P. Dewitt, Fundamentals of heat and mass transfer, Wiley, New York, 1990.
[29] R.C. Reid, J.M. Prausnitz, T.K. Sherwood. The Properties of Gases and Liquids, McGraw Hill, New York, 1977.
[30] R.H. Perry, C. Chilton, Chemical Engineer's Handbook, McGraw Hill, New York, 1973.
[31] B. Ozbas, Modeling of Asymmetric Membrane Formation by Dry-casting Method, MSc Thesis, Izmir Institute of Technology, Izmir, 2001.
[32] A.R. Greenberg, S.S. Shojaie, W.B. Krantz, S.B. Tantekin-Ersolmaz, Use of infrared thermography for temperature measurement during evaporative casting of thin polymeric films, J. Membr. Sci. 107 (1995) 249.